catalysts

MDPI

Article

Efficient Degradation of Refractory Organics Using Sulfate Radicals Generated Directly from WO_3 Photoelectrode and the Catalytic Reaction of Sulfate

Jingyuan Zheng [1], Jinhua Li [1], Jing Bai [1,*], Xiaohan Tan [1], Qingyi Zeng [1], Linsen Li [1] and Baoxue Zhou [1,2,*]

[1] School of Environmental Science and Engineering, Shanghai Jiao Tong University, No. 800 Dongchuan Road, Shanghai 200240, China; hjzhengjingyuan@sjtu.edu.cn (J.Z.); lijinhua@sjtu.edu.cn (J.L.); alissa@sjtu.edu.cn (X.T.); qingyizeng@126.com (Q.Z.); lilinsen@sjtu.edu.cn (L.L.)

[2] Key Laboratory of Thin Film and Microfabrication Technology, Ministry of Education, Shanghai 200240, China

* Correspondence: bai_jing@sjtu.edu.cn (J.B.); zhoubaoxue@sjtu.edu.cn (B.Z.); Tel.: +86-021-54747364 (J.B.); +86-021-54747351 (B.Z.)

Received: 12 October 2017; Accepted: 12 November 2017; Published: 17 November 2017

Abstract: An environment-friendly method of efficiently degrading refractory organics using $SO_4^{-}\bullet$ generated directly from a WO_3 photoelectrode and a catalytic reaction of sulfate was proposed, in which the cycling process of $SO_4^{2-} \rightarrow SO_4^{-}\bullet \rightarrow SO_4^{2-}$ was achieved in the treatment of organic pollutants without any other activator and without the continuous addition of sulfate. The results show that the removal efficiency for a typical refractory organics of methyl orange (MO) with 5 mg/L was up to 95% within 80 min, and merely 3% by photolysis and 19% by photocatalysis, respectively, under similar conditions. The rate constant for the disposal of MO at pH 2, in which $SO_4^{-}\bullet$ instead of HO• is the main oxidizer confirmed by radical scavenger experiment, is up to 5.21×10^{-4} s^{-1}, which was ~6.6 times that (7.89×10^{-5} s^{-1}) under neutral condition, in which HO• is the main oxidizer. The concentration of active persulfate ($S_2O_8^{2-}$, SO_5^{2-}, and $SO_4^{-}\bullet$) species at pH 2 was up to 0.38 mM, which was ~16-fold as much as that (0.023 mM) in neutral conditions. The method provides a new approach for the treatment and resource utilization of sulfate wastewater.

Keywords: sulfate radical; photoelectrocatalysis; WO_3; refractory organics; sulfate wastewater

1. Introduction

Peroxydisulfate ($S_2O_8^{2-}$), as a peroxide that possesses the highest oxidizability, can play a role in various chemical fields [1]. Recently, $S_2O_8^{2-}$ has received intense scrutiny in water purification and soil remediation since the activation of $S_2O_8^{2-}$ is one of the most effective methods of producing sulfate radical ($SO_4^{-}\bullet$) for the degradation of organic waste [2]. $SO_4^{-}\bullet$ with one unpaired electron has a high oxidation potential of 2.6~3.2 V vs. the normal hydrogen electrode (NHE), and more importantly has a longer lifetime (30–40 μs) than hydroxyl radical (HO•), so it is highly active to react with various contaminant, causing either partial or complete mineralization [3–5]. Currently, $SO_4^{-}\bullet$ is commonly produced from the activation of peroxydisulfate via heat [6–8], ultraviolet (UV) light [9,10], transition metals [11–13], or other means [14]. However, there are still some challenges for the application of $SO_4^{-}\bullet$ with these methods. The first problem is that a large amount of expensive peroxydisulfate must be used to form the highly reactive $SO_4^{-}\bullet$, leading to a high water treatment cost. The other is that the efficiency of activated persulfate in practical systems is relatively low because only one $SO_4^{-}\bullet$ from the activation of the peroxydisulfate can be obtained to oxidize organic compounds, and the other free radical was consumed by the activator, which might cause new secondary environment pollution. Therefore, how to cost-effectively produce and utilize $SO_4^{-}\bullet$ has become an urgent issue.

Photoelectrocatalytic (PEC) techniques as a promising advanced oxidization technology has attracted much attention in pollutant degradation because the photoelectrodes can generate free radicals under light illumination that can rapidly decompose organic compounds [15]. Some photoanode materials, such as TiO_2 [16–19], WO_3 [20–29], Fe_2O_3 [30,31], ZnO [32,33], and $BiVO_4$ [34–36] have been widely investigated because of their considerably high incident light-to-current conversion efficiencies. Among them, WO_3 is a promising material impacting many research fields [37] for its specific properties. For instance, it has a relatively narrow band gap of 2.5–2.7 eV, which can absorb approximately 12% of solar light with a theoretical maximum conversion efficiency of ~6.3%. Additionally, WO_3 possesses a moderate hole diffusion length (~150 nm) that is longer than those of α-Fe_2O_3 (2–4 nm) and TiO_2 (~100 nm), thus showing inherently good electron transport properties. Especially, the valence band edge of WO_3 is located at approximately 3.0 V vs. NHE [38], which provides a sufficient potential for the oxidation of sulfate to form $SO_4^{-}\bullet$ under visible light irradiation. This property gives us an inspiration that it is possible to find a new way to produce $SO_4^{-}\bullet$ using a WO_3 photoanode in a PEC system.

Refractory organics are usually difficult to decompose by organisms in natural conditions. Traditional treatment methods, such as biological methods and conventional physical and chemical methods, do not easily deal with refractory pollutants. This paper proposes a novel environmentally friendly method of efficiently degrading refractory organics using $SO_4^{-}\bullet$ generated directly from the catalysis of sulfate by a WO_3 photoelectrode, in which $SO_4^{-}\bullet$ can be favorably generated as a result of photocatalytic oxidation of sulfate, and a cycling process of $SO_4^{2-} \rightarrow SO_4^{-}\bullet \rightarrow SO_4^{2-}$ was achieved in the treatment of organic pollutants without the continuous addition of sulfate. $SO_4^{-}\bullet$ instead of HO• is the main oxidizer in the system, so the degradation of organics is mainly accomplished by $SO_4^{-}\bullet$, and no other activator needed to be added. In practice, a large amount of sulfate-rich wastewater is produced from medicine, chemical engineering, cement and dyeing, food, and fertilizer industries [39], which represents a potential threat to water ecological and human health [40]. Therefore, the proposed method provides a new way for the disposal and resource utilization of sulfate-rich organic wastewater.

2. Results and Discussion

2.1. Characterization of WO_3 Photoanodes

The obtained WO_3 films were transparent, uniform, and smooth on an F-doped tin oxide (FTO) substrate. Figure 1 shows a scanning electron microscope (SEM) image and an X-ray diffractometry (XRD) pattern of a typical WO_3 nanoplate array film. As is shown in Figure 1a, the prepared WO_3 films had platelike morphologies, and the average thickness of the plates was ~100 nm. The cross-sectional SEM images in Figure 1a show that the WO_3 films were perpendicular to the substrate and tightly adhered to the FTO substrate and the thickness of the WO_3 films remained almost the same at ~850 nm. Those results are in agreement with the reported [41]. Figure 1b shows the X-ray diffractometry (XRD) patterns of WO_3 nanoplate array films, where (020), (002), and (200) peaks were observed. The (020) and (002) diffraction peaks were relatively low, which indicates that the (020) direction and (002) direction were parallel to the substrate. Furthermore, the (200) direction was vertical to the substrate, as evidenced by the fact that the (200) peak exhibited the highest intensity.

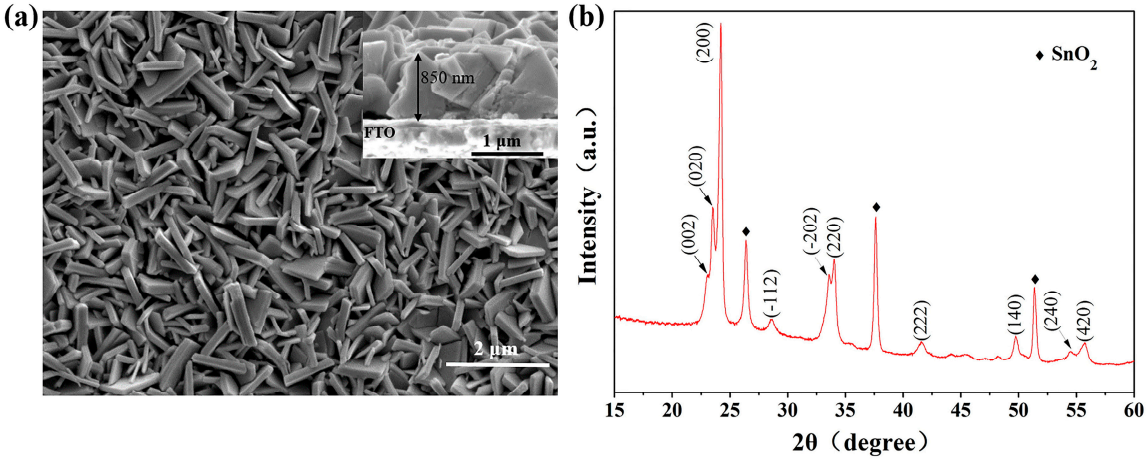


Figure 1. (**a**) The SEM images and (**b**) XRD patterns of the WO_3 nanoplate photoanode.

2.2. PEC Degradation of Methyl Orange in Sulfate Medium

Figure 2a shows the PEC degradation of 5 mg/L methyl orange (MO) within 80 min by photolysis, electrocatalysis (EC), photocatalysis (PC), and PEC in Na_2SO_4 solution (pH = 2, regulating the pH value with H_2SO_4), respectively. As can be seen, the photolytic reaction only resulted in a removal ratio of 3% within 80 min, and 18% of the MO was removed in electrocatalytic (EC) conditions at the same time. The photocatalytic reaction (without bias supply), compared to photolysis, degraded 19% of the MO within 80 min, while the PEC process obtained a removal rate of 95% under the same conditions. The significant advance of PEC over the other methods (photolysis and photocatalysis) is attributed to the electric bias that promoted the separation of photogenerated holes and electrons from recombination, and a more powerful oxidizer was probably produced in the PEC process.

Figure 2b shows the PEC degradation of 5 mg/L MO under different concentrations of Na_2SO_4 solution (0.1 M, 0.5 M, 0.7 M, 0.8 M, and 1 M) at pH = 2. Apparently, the removal rate of MO increased with the concentration of sulfate. Only 53% of methyl orange was removed in 0.1 M Na_2SO_4 within 80 min, while the removal rate reached a substantial level, 84%, 90%, and 95%, respectively, when the concentration of sulfate increased from 0.1 M to 0.5 M, 0.7 M, and 0.8 M (1 M). This result suggests that the concentration of sulfate has a direct effect on the degradation of methyl orange, indicating that the degradation of methyl orange is likely not attributed to hydroxyl radicals, but more likely new oxidizing species that are connected with sulfate. As is known, the valence band edge of WO_3 is located at approximately 3.0 V vs. NHE [38], theoretically, which could provide a sufficient potential to oxidize sulfate to $SO_4^{-}\bullet$ under visible light irradiation [1,38,42,43]. Furthermore, the preferential oxidation of HSO_4^- at WO_3/electrolyte contacts and the generation of peroxydisulfate ($S_2O_8^{2-}$) on a WO_3 photoanode in sulfuric acid was reported by Lewis et al. [42,43]. Therefore, we speculate that the fast degradation of methyl orange in 0.8 M Na_2SO_4 is possibly due to the active $SO_4^{-}\bullet$ generated on the WO_3 surface. With the increase of sulfate concentration, more sulfate oxidation occurred on WO_3 photoanondes [38,42,43] and water oxidation is suppressed. Thus, a large amount of $SO_4^{-}\bullet$ was produced such that the removal rate of MO was enhanced. Noting that, in 0.8 M and 1 M sulfate, removal rates were almost identical as shown in Figure 2b, the yield of $SO_4^{-}\bullet$ radicals reached the limit with over 0.8 M sulfate.

Figure 2c presents the degradation results of 5 mg/L MO measured at varying pH levels (pH 0, 1, 2, 3, and 7, the pH value being regulated with H_2SO_4). Obviously, the removal rate of MO was quicker at lower pH values. As can be seen, 95% of MO was degraded at pH 2.0, while the removal rate of MO was merely 32% at pH 7.0 over 80 min. It was also noted that the removal rate sharply increased as pH value decreased from 3.0 to 2.0. It was found that only 47% of MO was removed at pH 3.0, which is a small increment over the 32% under neutral condition (pH 7.0). However, there was a

100% and 200% increase in removal rate at 2.0 compared to that at 3.0 and 7.0, respectively, indicating that stronger acid conditions are favorable for the formation of $SO_4^{-}\bullet$. This is because the theoretical potential of water oxidation (Equation (1)) [43] is higher than that of sulfate oxidation under stronger acid conditions (pH < 2). The sulfate could be oxidized to form $SO_4^{-}\bullet$ in the PEC system, which subsequently promoted the removal of MO. With the increase in pH value (pH > 2), the potential of water oxidation continuously decreases, while the potential of sulfate oxidation was kept stable (Equation (2)) [1,44,45]. Therefore, water oxidation effectively competes with oxidation of sulfate at the WO_3/electrolyte interface and gradually dominates the photoanodic behavior of WO_3. In this case, the degradation of MO was hindered. Another phenomenon is that a further decreasing pH value (1, 0) did not show significant improvements in the removal rate of methyl orange. It is suggested that the yield of $SO_4^{-}\bullet$ on WO_3 electrodes reached a maximum level at pH 2.

$$2H_2O\ (l) \rightarrow O_2\ (g) + 4H^+\ (aq) + 4e^-. \quad (1)$$

$$2HSO_4^-\ (aq) \rightarrow S_2O_8^{2-}\ (aq) + 2H^+ + 2e^-. \quad (2)$$

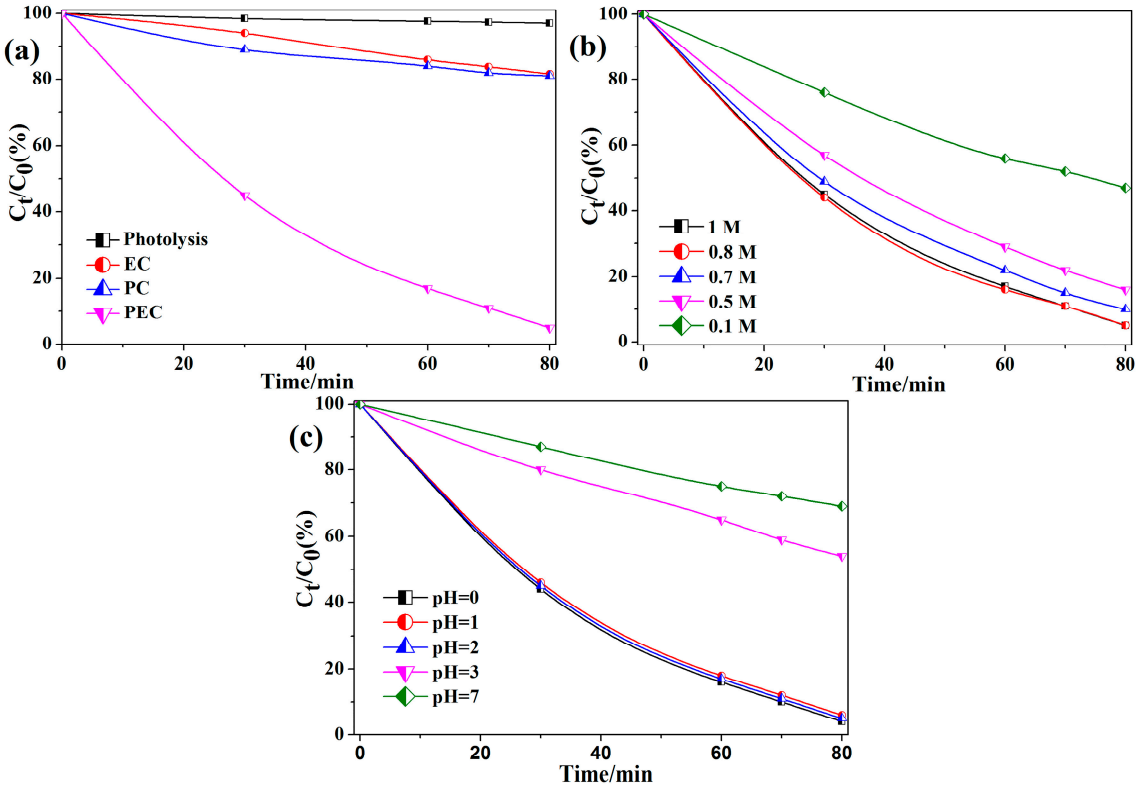


Figure 2. (**a**) The degradation of 5 mg/L methyl orange (MO) within 80 min by photolysis, photocatalysis, and PEC in 1 M Na_2SO_4 medium at pH = 2, respectively. (**b**) Removal of MO in a varying concentration of Na_2SO_4 aqueous solution (pH = 2) or (**c**) with different pH values (1 M Na_2SO_4). The initial conditions: MO 5 mg L^{-1}, applied 1.5 V vs. counter electrode (CE).

Additionally, degradation kinetics of MO by photoelectrocatalysis in different sulfate concentrations or in different pH value concentrations were investigated. The results show that the decolorization of MO followed the pseudo-first-order kinetic within 70 min, shown in Figure 3a, which can be expressed by Equation (3):

$$\ln(C_0/C_t) = kt \quad (3)$$

where k is the apparent reaction constant, and C_0 and C_t are the initial concentration and the concentration at time *t*, respectively. Consistent with results in Figure 2b, the apparent rate constant for the photoelectrocatalysis system reached the limit with over 0.8 M sulfate. The apparent rate constant in 1 M Na_2SO_4 was 5.20 × 10^{-4} s^{-1}, which was ~3.3 times that (1.58 × 10^{-4} s^{-1}) in 0.1 M Na_2SO_4.

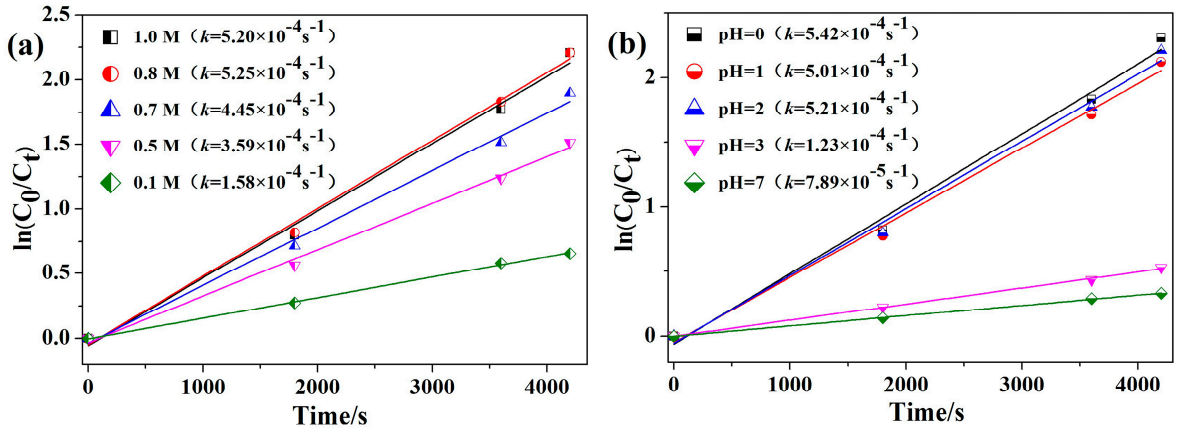


Figure 3. Plots of $\ln(C_0/C_t)$ versus time for the MO degradation (**a**) in different sulfate concentration or (**b**) in varying pH value (pH 0, 1, 2, 3, and 7).

Degradation kinetics of MO by photoelectrocatalysis in different pH value concentrations also obeyed pseudo-first-order kinetic within 70 min, shown in Figure 3b. The apparent rate constant at pH 2 is 5.21 × 10^{-4} s^{-1}, which was ~6.6 times that (7.89 × 10^{-5} s^{-1}) under neutral conditions.

2.3. Identification of Main Active Radical in the PEC System

As previously discussed, SO_4^{-}• could be the primary active species for the degradation of MO. However, hydroxyl radicals (HO•) originated from the oxidation of water by photogenerated holes is a common oxidant that can react with methyl orange in aqueous solution [43]. Therefore, the degradation of methyl orange in this study may have been achieved by SO_4^{-}• and HO•. In order to distinguish the effect of the two free radicals, excess methanol (MA) and *tert*-butyl alcohol (TBA) were added in the solution, respectively. Methanol is a well-known quenching agent for both sulfate and hydroxyl radicals, and reaction rate constant of methanol with sulfate radical is similar to that with hydroxyl radicals [46]. In contrast to MA, *tert*-butyl alcohol (TBA) with no alpha hydrogen is an effective quenching agent for hydroxyl radicals, which is 1000-fold faster than with sulfate radical [46,47].

Figure 4 presents the removal of MO in 1 M sulfate (pH = 2, 3, and 7) when the MA or TBA was added or not added, respectively. As is shown in Figure 4a, without any radical quenching agent, the removal rate of MO reached 95% but only 30% of MO was removed with the addition of 2 mM MA. This indicates that MA quenched almost all radicals in the solution so that redox was confined to the interface between electrode and electrolyte, thus greatly depressing the degradation of MO. Although the addition of TBA still hindered the degradation of MO, the removal rate increased to 57% compared to 30% with the use of MA. Since TBA is prone to react with hydroxyl radicals as previously mentioned, more SO_4^{-}• could be preserved and reacted with MO. This result confirmed that SO_4^{-}• might be the main oxidant resulting in the degradation of MO. It was noted that the removal rate was not more than 60% in 80 min. We speculated that TBA competed with sulfate for photoholes on WO_3 photoanode and that partial TBA could still react with SO_4^{-}•. As is shown in Figure 4b, the degradation of MO (30%) with an addition of 2 mM TBA was better than that (21%) with an addition of 2 mM MA at pH = 3, indicating that SO_4^{-}• still emerged in the WO_3 photoanode to react with MO. Under neutral conditions, shown in Figure 4c, the degradation of MO was greatly depressed by MA or TBA, indicating that hydroxyl radicals can be used as the main oxidant in the degradation of MO.

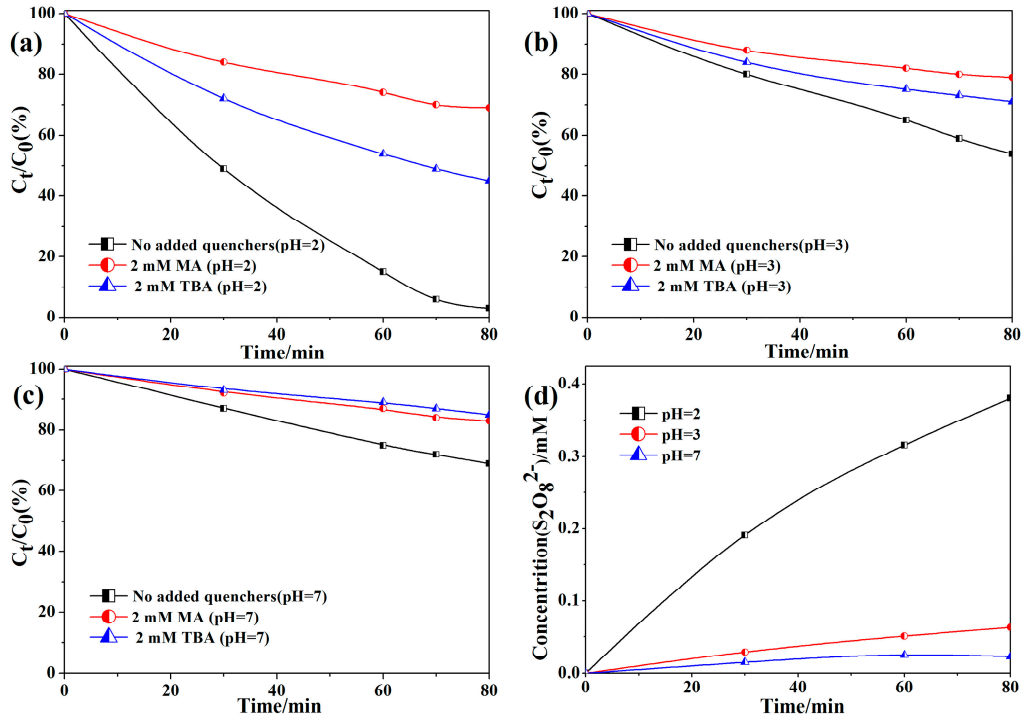


Figure 4. Removal of methyl orange with time and different additives to a 1.0 M Na_2SO_4 aqueous solution at (**a**) pH = 2. (**b**) pH = 3 and (**c**) pH = 7. The initial conditions: MO 5 mg L^{-1}, Na_2SO_4 1 M, applied 1.5 V vs. CE. (**d**) The concentration of $S_2O_8^{2-}$ with the function of time at different pH values (involving 40 mL of 1 M Na_2SO_4 aqueous solution).

SO_4^{-}• plays an important role in the degradation of MO, but it is difficult to direct identify the SO_4^{-}• in the whole process because of a short lifetime of sulfate radical. In fact, SO_4^{2-} can be oxidized to $S_2O_8^{2-}$ (Equation (2)) [43] and SO_4^{-}• could be an intermediate species that is prior to the formation of $S_2O_8^{2-}$ (Equation (4)). Therefore, the amount of SO_4^{-}• could be indirectly analyzed by investigating the production of $S_2O_8^{2-}$. In fact, a small part of $S_2O_8^{2-}$ in 1.0 M Na_2SO_4 was hydrolyzed to produce HSO_5^{-}, which has an effect on the determination of $S_2O_8^{2-}$ via colorimetry, but the hydrolysis of $S_2O_8^{2-}$ is so slow that it can be neglected [43]. Thus, we assumed here that the concentration of $S_2O_8^{2-}$ was also equal to the total active persulfate ($S_2O_8^{2-}$, SO_5^{2-}, SO_4^{-}•) species, which can be represented by the result determined by colorimetry.

$$2SO_4^{2-} + 2h^+ \rightarrow 2\,SO_4^{-}\bullet \rightarrow S_2O_8^{2-}. \quad (4)$$

Figure 4d shows the concentration of $S_2O_8^{2-}$ with time in various pH values. At different pH values, the amount of $S_2O_8^{2-}$ maintains a steady rise, indicating that the yield of $S_2O_8^{2-}$ remains relatively constant and decreases gradually over time at the same pH value within 80 min. Simultaneously, pH values have a great effect on the generation of $S_2O_8^{2-}$. The amount of $S_2O_8^{2-}$ rapidly decreased as pH increased, which suggests that the photoholes on the surface of the WO_3 photoanode tended to oxidize water molecules (Equation (1)) instead of the sulfate anion at high pH values [38].

In order to further confirm the preferential formation of $S_2O_8^{2-}$ in strong acidic conditions, the photoconversion efficiency for the different species was investigated. According to the I–V curves of the WO_3 photoanode in the PEC process, the photoconversion efficiency can be calculated by Equation (5) [1,43]:

$$\text{Photoconversion efficiency} = \frac{J\left(\text{E}\left(\frac{\text{A}}{\text{A}^-}\right) - E\right) \times \text{faraday efficiency}}{\text{In}t} \times 100 \quad (5)$$

where *J* is the photocurrent density, Int is the illumination power density, *E* is the applied photoanode potential, A^- represent a reduced species (H_2O or HSO_4^-), A represent an oxidized species (O_2 or $S_2O_8^{2-}$), E(O_2/H_2O) is 1.23 V vs. NHE and E($S_2O_8^{2-}/HSO_4^-$) is 2.12 V.

As shown in Figure 5a, the photocurrent of the WO_3 photoanode reached 2.8 mA cm^{-2} at 2.1 V vs. counter electrode in 1.0 M Na_2SO_4 solution at pH 2. In this case, the photoconversion efficiency for $S_2O_8^{2-}$ reached a maximum of 2.16% at 1.2 V vs. counter electrode (Figure 5b). However, given that O_2 (g) was the product in the WO_3 photoanode, the photoconversion efficiency would merely yield a maximum 0.39% at 0.96 V vs. counter electrode. This suggests that solar light energy, compared to the oxidation of water, is better utilized for the production of $S_2O_8^{2-}$ in strong acidic conditions, which is consistent with the trend of MO degradation.

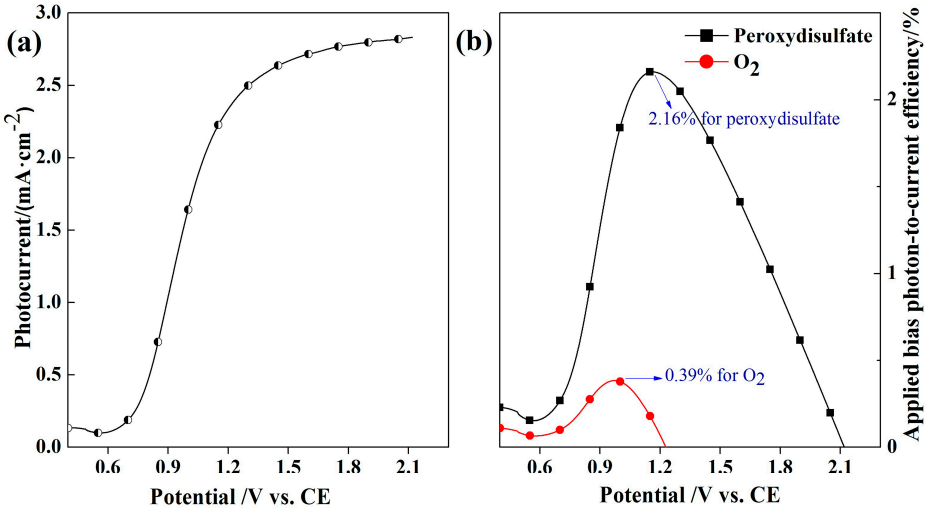


Figure 5. (**a**) The photocurrent and (**b**) the applied bias photo-current efficiency in a 1.0 M Na_2SO_4 aqueous solution (pH = 2) by using a WO_3 photoanode under illumination of simulated solar light.

2.4. The PEC Degradation Mechanism of MO

Theoretically, SO_4^{2-} can be oxidized to $S_2O_8^{2-}$ (Equation (2)) in a WO_3 photoanode at any pH value. However, the theoretical voltage of water oxidation to form O_2 (Equation (1)) is affected by the concentration of hydrogen ions. The high pH value (pH > 2) is conducive to the evolution of oxygen from water oxidation. Equation (1) dominates the oxidative processes at WO_3 photoanodes in 1.0 M Na_2SO_4 at high pH values (pH > 2). This is consistent with the low production of $S_2O_8^{2-}$ when pH is 3 or 7, shown in Figure 6. Therefore, at a high pH value (pH > 2), the decolorization of methyl orange can be attributed to hydroxyl radical (HO•) from water oxidation by photogenerated holes (h^+) via the following equations:

$$H_2O + h^+ \rightarrow HO\bullet + H^+ \quad (6)$$

$$MO + HO\bullet \rightarrow \text{products} + H_2O. \quad (7)$$

Sulfate, instead of water, was oxidized by photogenerated holes (h^+) at low pH levels. A reasonable schematic mechanism for efficiently removing MO using a WO_3 electrode in a PEC system is shown in Figure 6. The production of $S_2O_8^{2-}$ at pH 2 is approximately six times that at pH 3. Prior to the peroxydisulfate ($S_2O_8^{2-}$), the photogenerated $SO_4^-\bullet$ can initially be formed as intermediates in the WO_3 photoanode [42,48]. Subsequently, the generated $SO_4^-\bullet$ can directly react with MO in Na_2SO_4 solution and revert to SO_4^{2-} (Equations (8) and (9)). Additionally, from the dynamic viewpoint, the existence

of hydrogen ion is beneficial to the oxidation of $SO_4^{-}\bullet$ to form HSO_4^{-} in the case of low pH, which accelerates the reaction between sulfate radical and organic compounds.

$$SO_4^{2-} + h^+ \rightarrow SO_4^{-}\bullet \quad (8)$$

$$MO + SO_4^{-}\bullet \rightarrow products + HSO_4^{-} \quad (9)$$

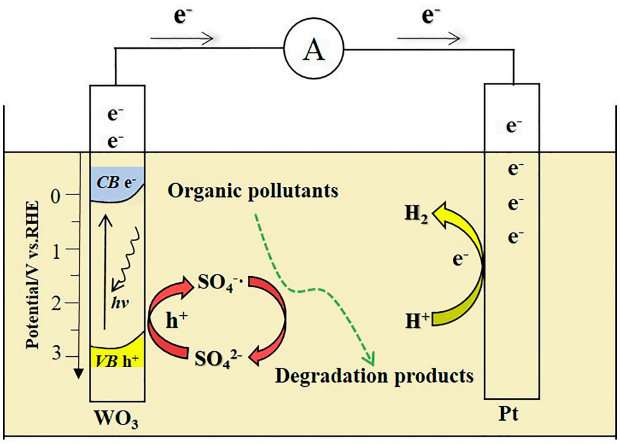


Figure 6. Schematic illustration of efficiently degrading MO with WO_3 electrode in Na_2SO_4.

2.5. Recycling Performance

For environmental applications, the long-term operation of the PEC system is also a key property. According to the above assumption, firstly, SO_4^{2-} transforms into $SO_4^{-}\bullet$, and $SO_4^{-}\bullet$ can react with MO and be reduced to SO_4^{2-}. Therefore, the SO_4^{2-} undergoes a cycle in the oxidation process. With these considerations in mind, we expected that MO can be continuously degraded in the proposed PEC method. Figure 7 shows three successive MO degradation experiments using a WO_3 photoanode in 1 M Na_2SO_4 (pH = 2). At 80 min intervals, 5 mg L^{-1} MO was added to the system again without additional SO_4^{2-}. It can be seen from Figure 7 that MO degradation efficiency in the three tests were 95%, 94%, and 95%, respectively. In other words, MO can be continuously removed in this PEC system without adding chemical additives.

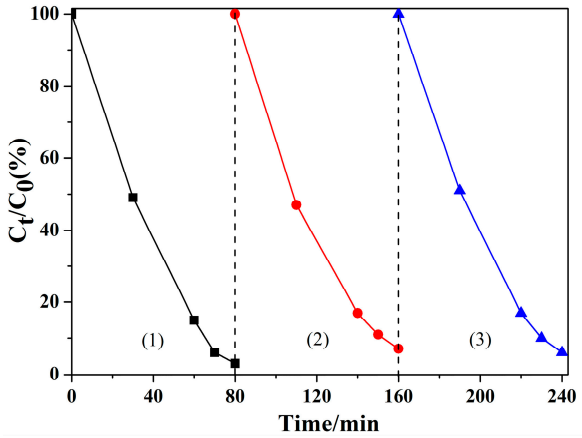


Figure 7. MO degradation during a series of three tests with additional 5 mg L^{-1} MO at 80 min intervals. The initial conditions: MO 5 mg L^{-1}, Na_2SO_4 1 M L^{-1}, applied 1.5 V vs. CE and pH = 2.

3. Materials and Methods

3.1. Chemicals

Sodium tungstate ($Na_2WO_4 \cdot 2H_2O$), oxalic acid($H_2C_2O_4$), carbamide ($CO(NH_2)_2$), hydrogen peroxide (H_2O_2, 30%), sodium sulfate (Na_2SO_4), ferrous (II) sulfate ($FeSO_4$), methyl orange (MO) and sulphuric acid (H_2SO_4, 98%) were purchased from Sinopharm Chemical Reagent Co. Ltd. (Shanghai, China). Hydrochloric acid (HCl, 37%) was purchased in Shanghai Lingfeng Chemical Reagent Co., Ltd. (Shanghai, China). The needed water used during the whole work was deionized (DI) water produced by a Milli-Q ultrapure water system (Millipore, Burlington, MA, USA).

3.2. Preparation of WO_3 Photoanodes

The WO_3 photoanodes used in this work were prepared using a method reported elsewhere [41]. In a typical process, the SnO_2:F-coated glass slides (FTO) of 3 × 3 cm was pretreated by washing it under ultrasonication with acetone and deionized water for 30 min. A standard precursor solution was prepared as follows. Firstly, 0.4 g of $Na_2WO_4 \cdot 2H_2O$, 0.08 g of $H_2C_2O_4$, and 0.16 g $CO(NH_2)_2$ were dissolved in 33 mL of deionized water (pH 8.6), and 9 mL of HCl (37%) was added to this solution with strong agitation for about 1 min to form a suspension. Then, 8 mL of H_2O_2 (37%) was added into this suspension with strong agitation for 10 min to form a clear solution. Last, 30 mL of ethanol was added with more strong agitation for 10 min to obtain a clear and stable solution. The FTO glass after pretreatment was dipped into precursor solution with the FTO side facing down. The synthesis was carried out at 94 °C in a constant temperature heating device for 240 min and then allowed to cool naturally. Then, the as-prepared film was rinsed with deionized water for 1 min and dried at 50 °C for 10 h. Next, the as-prepared film was annealed in a muffle at 500 °C for 2 h and a cooling rate of 1 °C/min to obtain WO_3 photoanodes.

3.3. Apparatus and Methods

The morphologies and microstructures of WO_3 photoanodes were performed by FE-SEM (Sirion200, Philips, Amsterdam, The Netherlands). The crystal phase of the samples was characterized with X-ray diffractometry (XRD) (AXS-8 Advance, Bruker, Karlsruhe, Germany). In a two electrode system, linear sweep voltammetry for WO_3 films photocurrent measurements was investigated under 100 mW cm^{-2} simulated sunlight from an Xe lamp in 1.0 M Na_2SO_4 (pH = 2) at 0.4 – 2.12 V vs. counter electrode.

A photoelectrocatalysis (PEC) system was constructed using an as-prepared nano-WO_3 photoanode and a Pt-black cathode in Na_2SO_4 solution under light illumination for the degradation of 5 mg/L MO. All of the photoelectrochemical experiments of MO degradation were performed at 1.5 V of bias voltage, in 50 mL of a quartz glass reactor containing 40 mL of sodium sulfate electrolyte, with only approximately 1 cm^2 WO_3 photoanodes exposed to under 100 mW cm^{-2} AM1.5G simulated sunlight from an Xe lamp. The degradation of 5 mg/L MO within 80 min by photolysis, electrocatalysis (EC), photocatalysis, and PEC in Na_2SO_4 medium were investigated. The photolysis experiment was carried out to determine the degradation rate of MO only under visible light irradiation. The electrocatalysis (EC) experiment was performed in a photoelectrocatalysis system, where 1.5 V vs. counter electrode of bias voltage was applied to the WO_3/FTO electrode in darkness. The photocatalysis (PC) experiment was performed in photoelectrocatalysis system but with no bias voltage compared with photoelectrocatalysis. The effects of sulfate concentrations and pH value on the degradation of methyl orange were also investigated in this photoelectrocatalytic system. Active species resulting in the catalytic oxidation of MO was identified. In addition, the practical ability of the photoelectrochemical system to yield active persulfate ($S_2O_8^{2-}$, SO_5^{2-}, and $SO_4^{-}\bullet$) species was evaluated according to the production of peroxydisulfate ($S_2O_8^{2-}$). The peroxydisulfate ($S_2O_8^{2-}$) quantity was measured by colorimetry using UV-VIS spectroscopy at 310 nm in 1 M sodium sulfate solution with different pH values. The sample solution was stirred with an equivalent amount of 0.01 M

$FeSO_4$ and 1 M H_2SO_4 solution to measure the optical absorbance spectra at 310 nm, and concentration was evaluated according standard curve [49].

4. Conclusions

In this paper, a novel green method was successfully established to highly efficiently remove refractory organics using SO_4^{-}• generated directly from a WO_3 photoelectrode and the catalytic reaction of sulfate without the addition of any other activator. The results show that the removal efficiency for MO with 5 mg/L was up to 95% within 80 min in the PEC system, and merely 3% by photolysis and 19% by photocatalysis, respectively, under similar conditions. The rate constant for the disposal of MO at pH 2, in which SO_4^{-}• instead of HO• was the main oxidizer, confirmed by a radical scavenger test, was up to 5.21×10^{-4} s^{-1}, which was ~6.6 times that (7.89×10^{-5} s^{-1}) under neutral conditions, in which HO• was the main oxidizer. Additional, the concentration of active persulfate ($S_2O_8^{2-}$, SO_5^{2-}, SO_4^{-}•) species at pH 2 was up to 0.38 mM, which was ~16 times that in neutral conditions (0.023 mM). The proposed method could be a new, effective, environmentally friendly approach for the treatment and resource utilization of sulfate wastewater.

Acknowledgments: The authors would like to acknowledge the National Nature Science Foundation of China (51578332, 21576162, No. 21507085) and SJTU-AEMD for support.

Author Contributions: Jingyuan Zheng, Baoxue Zhou, Jing Bai, and Qingyi Zeng conceived and designed the experiments; Jingyuan Zheng and Xiaohan Tan performed the experiments; Jingyuan Zheng, Baoxue Zhou, Jing Bai, Linsen Li, and Jinhua Li analyzed the data; Jingyuan Zheng wrote the paper. Baoxue Zhou and Jing Bai participated in writing the paper.

Conflicts of Interest: The authors declare no conflict of interest.

References

1. Fuku, K.; Wang, N.; Miseki, Y.; Funaki, T.; Sayama, K. Photoelectrochemical reaction for the efficient production of hydrogen and high-value-added oxidation reagents. *ChemSusChem* **2015**, *8*, 1593–1600. [CrossRef] [PubMed]
2. Huang, Y.; Wang, Z.; Fang, C.; Liu, W.; Lou, X.; Liu, J. Importance of reagent addition order in contaminant degradation in an Fe(II)/PMS system. *RSC Adv.* **2016**, *6*, 70271–72026. [CrossRef]
3. Anipsitakis, G.P.; Dionysiou, D.D. Radical generation by the interaction of transition metals with common oxidants. *Environ. Sci. Technol.* **2004**, *38*, 3705–3712. [CrossRef] [PubMed]
4. Mi, Z.; Chen, X.; He, Z.; Murugananthan, M.; Zhang, Y. Degradation of p-nitrophenol by heat and metal ions co-activated persulfate. *Chem. Eng. J.* **2015**, *264*, 39–47.
5. Wang, C.W.; Liang, C. Oxidative degradation of TMAH solution with UV persulfate activation. *Chem. Eng. J.* **2014**, *254*, 472–478. [CrossRef]
6. Huang, K.C.; Zhao, Z.; Hoag, G.E.; Dahmani, A.; Block, P.A. Degradation of volatile organic compounds with thermally activated persulfate oxidation. *Chemosphere* **2005**, *61*, 551–560. [CrossRef] [PubMed]
7. Waldemer, R.H.; Tratnyek, P.G.; Johnson, R.L.; Nurmi, J.T. Oxidation of chlorinated ethenes by heat-activated persulfate: Kinetics and products. *Environ. Sci. Technol.* **2007**, *41*, 1010–1015. [CrossRef] [PubMed]
8. Zhang, Y.Q.; Du, X.Z.; Huang, W.L. Temperature effect on the kinetics of persulfate oxidation of p-chloroaniline. *Chin. Chem. Lett.* **2011**, *22*, 358–361. [CrossRef]
9. Criquet, J.; Leitner, N.K.V. Degradation of acetic acid with sulfate radical generated by persulfate ions photolysis. *Chemosphere* **2009**, *77*, 194–200. [CrossRef] [PubMed]
10. Saien, J.; Ojaghloo, Z. Homogeneous and heterogeneous AOPs for rapid degradation of Triton X-100 in aqueous media via UV light, nano titania hydrogen peroxide and potassium persulfate. *Chem. Eng. J.* **2011**, *167*, 172–182. [CrossRef]
11. Do, S.H.; Kwon, Y.J.; Kong, S.H. Effect of metal oxides on the reactivity of persulfate/Fe(II) in the remediation of diesel-contaminated soil and sand. *J. Hazard. Mater.* **2010**, *182*, 933–936. [CrossRef] [PubMed]
12. Xu, X.; Ye, Q.; Tang, T.; Wang, D. Hg^0 oxidative absorption by $K_2S_2O_8$ solution catalyzed by Ag^+ and Cu^{2+}. *J. Hazard. Mater.* **2008**, *158*, 410–416. [CrossRef] [PubMed]

13. Xu, X.R.; Li, X.Z. Degradation of azo dye Orange G in aqueous solutions by persulfate with ferrous ion. *Sep. Purif. Technol.* **2010**, *72*, 105–111. [CrossRef]
14. Yuchi, L.; Shanglien, L.; Peite, C.; Chang, D.G. Efficient decomposition of perfluorocarboxylic acids in aqueous solution using microwave-induced persulfate. *Water Res.* **2009**, *43*, 2811–2816.
15. Bai, J.; Zhou, B. Titanium Dioxide Nanomaterials for Sensor Applications. *Chem. Rev.* **2014**, *114*, 10131–10176. [CrossRef] [PubMed]
16. Chen, P.; Wang, F.; Chen, Z.F.; Zhang, Q.; Su, Y.; Shen, L.; Yao, K.; Liu, Y.; Cai, Z.; Lv, W.; et al. Study on the photocatalytic mechanism and detoxicity of gemfibrozil by a sunlight-driven TiO_2/carbon dots photocatalyst: The significant roles of reactive oxygen species. *Appl. Catal. B* **2017**, *204*, 250–259. [CrossRef]
17. Fang, W.; Xing, M.; Zhang, J. Modifications on reduced titanium dioxide photocatalysts: A review. *J. Photochem. Photobiol. C Photochem. Rev.* **2017**, *32*, 21–39. [CrossRef]
18. Antoniadou, M.; Lianos, P. Production of electricity by photoelectrochemical oxidation of ethanol in a PhotoFuelCell. *Appl. Catal. B* **2010**, *99*, 307–313. [CrossRef]
19. Pop, L.C.; Sfaelou, S.; Lianos, P. Cation adsorption by mesoporous titania photoanodes and its effect on the current-voltage characteristics of photoelectrochemical cells. *Electrochim. Acta* **2015**, *156*, 223–227. [CrossRef]
20. Song, X.N.; Wang, C.Y.; Wang, W.K.; Zhang, X.; Hou, N.N.; Yu, H.Q. A Dissolution-Regeneration Route to Synthesize Blue Tungsten Oxide Flowers and their Applications in Photocatalysis and Gas Sensing. *Adv. Mater. Interfaces* **2016**, *3*. [CrossRef]
21. Altomare, M.; Pfoch, O.; Tighineanu, A.; Kirchgeorg, R.; Lee, K.; Selli, E.; Schmuki, P. Molten *o*-H_3PO_4: A New Electrolyte for the Anodic Synthesis of Self-Organized Oxide Structures: WO_3 Nanochannel Layers and Others. *J. Am. Chem. Soc.* **2015**, *137*, 5646–5649. [CrossRef] [PubMed]
22. Kalanur, S.S.; Yun, J.H.; Sang, Y.C.; Joo, O.S. Facile growth of aligned WO_3 nanorods on FTO substrate for enhanced photoanodic water oxidation activity. *J. Mater. Chem. A* **2013**, *1*, 3479–3488. [CrossRef]
23. Kim, Y.O.; Yu, S.H.; Ahn, K.S.; Lee, S.K.; Kang, S.H. Photoelectrochemical Behavior of Compact and Inverse Opal Tungsten Trioxide Films: Surface Area and Charge Transfer Properties. *J. Electrochem. Soc.* **2015**, *162*, H449–H452. [CrossRef]
24. Li, W.; Da, P.; Zhang, Y.; Wang, Y.; Lin, X.; Gong, X.; Zheng, G. WO_3 Nanoflakes for Enhanced Photoelectrochemical Conversion. *ACS Nano* **2014**, *8*, 11770–11777. [CrossRef] [PubMed]
25. Rao, P.M.; Cho, I.S.; Zheng, X. Flame synthesis of WO_3 nanotubes and nanowires for efficient photoelectrochemical water-splitting. *Proc. Combust. Inst.* **2013**, *34*, 2187–2195. [CrossRef]
26. Smith, Y.R.; Sarma, B.; Mohanty, S.K.; Misra, M. Formation of TiO_2-WO_3 nanotubular composite via single-step anodization and its application in photoelectrochemical hydrogen generation. *Electrochem. Commun.* **2012**, *19*, 131–134. [CrossRef]
27. Thind, S.S.; Rozic, K.; Amano, F.; Chen, A. Fabrication and photoelectrochemical study of WO_3-based bifunctional electrodes for environmental applications. *Appl. Catal. B* **2015**, *176*, 464–471. [CrossRef]
28. Yang, J.; Zhang, X.; Liu, H.; Wang, C.; Liu, S.; Sun, P.; Wang, L.; Liu, Y. Heterostructured TiO_2/WO_3 porous microspheres: Preparation, characterization and photocatalytic properties. *Catal. Today* **2013**, *201*, 195–202. [CrossRef]
29. Zheng, J.Y.; Song, G.; Hong, J.; Van, T.K.; Pawar, A.U.; Kim, D.Y.; Chang, W.K.; Haider, Z.; Kang, Y.S. Facile Fabrication of WO_3 Nanoplates Thin Films with Dominant Crystal Facet of (002) for Water Splitting. *Cryst. Growth Des.* **2014**, *14*, 6057–6066. [CrossRef]
30. Wang, G.; Ling, Y.; Wheeler, D.A.; George, K.E.; Horsley, K.; Heske, C.; Zhang, J.Z.; Li, Y. Facile synthesis of highly photoactive α-Fe_2O_3-based films for water oxidation. *Nano Lett.* **2011**, *11*, 3503–3509. [CrossRef] [PubMed]
31. Zeng, Q.; Bai, J.; Li, J.; Xia, L.; Huang, K.; Li, X.; Zhou, B. A novel in situ preparation method for nanostructured a-Fe_2O_3 films from electrodeposited Fe films for efficient photoelectrocatalytic water splitting and the degradation of organic pollutants. *J. Mater. Chem. A* **2015**, *3*, 4345–4353. [CrossRef]
32. Yousefi, M.; Amiri, M.; Azimirad, R.; Moshfegh, A.Z. Enhanced photoelectrochemical activity of Ce doped ZnO nanocomposite thin films under visible light. *J. Electroanal. Chem.* **2011**, *661*, 106–112. [CrossRef]
33. Zhao, Q.D.; Wang, D.J.; Peng, L.L.; Lin, Y.H.; Yang, M.; Xie, T.F. Surface photovoltage study of photogenerated charges in ZnO nanorods array grown on ITO. *Chem. Phys. Lett.* **2007**, *434*, 96–100. [CrossRef]

34. Sayama, K.; Nomura, A.; Arai, T.; Sugita, T.; Abe, R.; Yanagida, M.; Oi, T.; Iwasaki, Y.; Abe, Y.; Sugihara, H. Photoelectrochemical decomposition of water into H_2 and O_2 on porous $BiVO_4$ thin-film electrodes under visible light and significant effect of Ag ion treatment. *J. Phys. Chem. B* **2006**, *110*, 11352–11360. [CrossRef] [PubMed]
35. Yu, J.; Kudo, A. Effects of Structural Variation on the Photocatalytic Performance of Hydrothermally Synthesized $BiVO_4$. *Adv. Funct. Mater.* **2006**, *16*, 2163–2169. [CrossRef]
36. Zhang, X.; Du, L.; Wang, H.; Dong, X.; Zhang, X.; Ma, C.; Ma, H. Highly ordered mesoporous $BiVO_4$: Controllable ordering degree and super photocatalytic ability under visible light. *Microporous Mesoporous Mater.* **2013**, *173*, 175–180. [CrossRef]
37. Zheng, H.; Ou, J.Z.; Strano, M.S.; Kaner, R.B.; Mitchell, A.; Kalantar-Zadeh, K. Nanostructured Tungsten Oxide—Properties, Synthesis, and Applications. *Adv. Funct. Mater.* **2011**, *21*, 2175–2196. [CrossRef]
38. Hill, J.C.; Choi, K.S. Effect of Electrolytes on the Selectivity and Stability of n-type WO_3 Photoelectrodes for Use in Solar Water Oxidation. *J. Phys. Chem. C* **2012**, *116*, 7612–7620. [CrossRef]
39. Ghigliazza, R.; Lodi, A.; Rovatti, M. Kinetic and process considerations on biological reduction of soluble and scarcely soluble sulfates. *Resour. Conserv. Recycl.* **2000**, *29*, 181–194. [CrossRef]
40. Benatti, C.T.; Tavares, C.R.; Lenzi, E. Sulfate removal from waste chemicals by precipitation. *J. Environ. Manag.* **2009**, *90*, 504–511. [CrossRef] [PubMed]
41. Zeng, Q.; Li, J.; Bai, J.; Li, X.; Xia, L.; Zhou, B. Preparation of vertically aligned WO_3 nanoplate array films based on peroxotungstate reduction reaction and their excellent photoelectrocatalytic performance. *Appl. Catal. B* **2017**, *202*, 388–396. [CrossRef]
42. Mi, Q.; Coridan, R.H.; Brunschwig, B.S.; Gray, H.B.; Lewis, N.S. Photoelectrochemical oxidation of anions by WO_3 in aqueous and nonaqueous electrolytes. *Energy Environ. Sci.* **2013**, *6*, 2646–2653. [CrossRef]
43. Mi, Q.; Zhanaidarova, A.; Brunschwig, B.S.; Gray, H.B.; Lewis, N.S. A quantitative assessment of the competition between water and anion oxidation at WO_3 photoanodes in acidic aqueous electrolytes. *Energy Environ. Sci.* **2012**, *5*, 5694–5700. [CrossRef]
44. Kelsall, G.H.; Thompson, I. Redox Chemistry of H_2S Oxidation in the British-Gas Stretford Process 1: Thermodynamics of Sulfur-Water Systems at 298 K. *J. Appl. Electrochem.* **1993**, *23*, 279–286. [CrossRef]
45. Murray, R.C.; Cubicciotti, D. Thermodynamics of Aqueous Sulfur Species to 300 °C and Potential-pH Diagrams. *J. Electrochem. Soc.* **1983**, *130*, 866–869. [CrossRef]
46. Anipsitakis, G.P.; Dionysiou, D.D. Degradation of organic contaminants in water with sulfate radicals generated by the conjunction of peroxymonosulfate with cobalt. *Environ. Sci. Technol.* **2003**, *37*, 4790–4797. [CrossRef] [PubMed]
47. Buxton, G.V.; Greenstock, C.L.; Helman, W.P.; Ross, A.B. Critical Review of rate constants for reactions of hydrated electrons, hydrogen atoms and hydroxyl radicals ($\cdot OH/\cdot O^-$) in Aqueous Solution. *J. Phys. Chem. Ref. Data* **1988**, *17*, 513–886. [CrossRef]
48. Solarska, R.; Santato, C.; Jorand-Sartoretti, C.; Ulmann, M.; Augustynski, J. Photoelectrolytic oxidation of organic species at mesoporous tungsten trioxide film electrodes under visible light illumination. *J. Appl. Electrochem.* **2005**, *35*, 715–721. [CrossRef]
49. Nakajima, T.; Hagino, A.; Nakamura, T.; Tsuchiya, T.; Sayama, K. WO_3 nanosponge photoanodes with high applied bias photon-to-current efficiency for solar hydrogen and peroxydisulfate production. *J. Mater. Chem. A* **2016**, *4*, 17809–17818. [CrossRef]



© 2017 by the authors. Licensee MDPI, Basel, Switzerland. This article is an open access article distributed under the terms and conditions of the Creative Commons Attribution (CC BY) license (http://creativecommons.org/licenses/by/4.0/).